Journal of
Water & Climate Change

IWA PUBLISHING

Journal of Water and Climate Change Vol 13 No 3, 1599 doi: 10.2166/wcc.2021.247

Remote sensing inversion characteristic and driving factor analysis of wetland evapotranspiration in the Sanmenxia Reservoir area, China

Shiyan Wang*, Chang Liu, Yiqian Tan, Jie Wang, Fei Du, Zhen Han, Zhi Jiang and Liang Wang

State Key Laboratory of Simulation and Regulation of Water Cycle in River Basin, and Department of Water Ecology and Environment, China Institute of Water Resources and Hydropower Research, Beijing 100038, China
*Corresponding author. E-mail: shiyan_wang188@outlook.com

ABSTRACT

Evapotranspiration in the hydrologic cycle realizes the energy and water transport in the atmosphere. Evapotranspiration differences concerning land-use types provide data for studying the evapotranspiration of river basins. To investigate the evapotranspiration in the reservoir under artificial regulation, we selected the river basin in the Sanmenxia Reservoir as the study area. Data sources are two-period Landsat8 OIL_TIRS remote sensing images during the growing season of wetland plants. Based on meteorological data in this river basin, we investigated the evapotranspiration differences of different land-use types using the Surface Energy Balance Algorithm for Land model. The FAO Penman–Monteith formula verified the remote sensing inversion results. Analysis shows that significant differences were manifested between wetland and non-wetland landscapes in evapotranspiration among different land-use types. Non-wetland landscapes accounted for about 97.23% of the river basin's total area, but their daily average evapotranspiration was only 7.26 mm/d. Those of wetland landscapes were 2.77% and 12.17 mm/d. In this river basin, the differences between the wetland and non-wetland landscapes in evapotranspiration are mainly associated with plant diversity, vegetation coverage and surface temperature (beyond other driving factors like meteorological and hydrological solar radiation factors).

Key words: evapotranspiration, land utilization, river basin in Sanmenxia Reservoir area, SEBAL model, wetland

HIGHLIGHTS

- Evapotranspiration data of different land types that support study on the hydrological cycle process in the watershed.
- SEBAL model based on satellite remote sensing data and geographic information system technology.
- The model simulation results have been verified by the Penman–Monteith formula.

1. INTRODUCTION

The global hydrologic cycle is greatly affected by climate change. The hydrologic cycle links surface processes and atmospheric processes. It realizes the dynamic circulation of solid, liquid and gaseous water through various physical forms (e.g., precipitation, runoff and evapotranspiration) and regulates global water resources' spatial and temporal patterns. Moreover, the hydrologic cycle plays a vital role in forming, developing and succession of wetlands. Evapotranspiration, a key process in the hydrologic cycle, enables the transfer of energy and water on the land surface and in the atmosphere (Wu 2016) and accelerates the succession of wetland ecosystems while facilitating the hydrologic cycle. The wetland ecosystem, one of three major global ecosystems (forest and ocean), provides the carrier of material conversion for the evapotranspiration process.

Moreover, wetlands play irreplaceable roles in climate regulation, pollutant degradation and floodwater storage by constituting a unique ecosystem formed under the water and land interaction. Therefore, the research on the evolution patterns of wetland evapotranspiration is a significant part of the research on the global hydrologic cycle due to its particularity, importance and complexity. The accurate estimation of evaporation capacity would be useful for drought monitoring and evaluation, wetland vegetation growth, crop water demand and production management, soil moisture status monitoring and groundwater level monitoring.

With the development and perfection of satellite remote sensing and geographic information system technology, the limitations of the traditional point measurement method have been resolved by introducing remote sensing data into the

evapotranspiration model and combining it with meteorological data, thus realizing the 'point-to-plane' conversion of evapotranspiration estimation. Evapotranspiration research is developing in the direction of combining experimental science with theoretical science. In the 1960s, handheld infrared thermometer was used for the first time to measure crop temperature and evaluate crop growth status. The measured temperature value could be affected by crop structure (vegetation coverage, leaf area index, crop height and surface roughness), light condition (azimuth angle and elevating angle) and observation angle. For a long time, evaporation research has been mainly at the site scale measured by evaporation instruments. In the 1970s, the thermal infrared image data generated by satellite-borne thermal infrared scanner was also applied to calculate the difference between brightness temperature and air temperature (Allen *et al.* 1998). Bastiaanssen developed the Surface Energy Balance Algorithm for Land (SEBAL) to calculate latent heat flux and estimate the actual evapotranspiration, evaporation ratio and surface impedance in the Mediterranean region. He reported that the surface impedance was closely correlated with the surface soil moisture content, but the correlation varied with the spatial and temporal changes. After a correction through field experiment, the correlation between the surface impedance and surface soil moisture content could be used to estimate the soil moisture content in other regions (Bastiaanssen 1995). Based on Landsat and observed meteorological data, Liu *et al.* (2020) utilized the SEBAL model to estimate the spatial and temporal patterns of wetland evapotranspiration in the Liaohe River Delta in the growing season. Zheng *et al.* (2020) explored the evapotranspiration in the Jinghe River basin based on the SEBS model. The methods proposed and optimized as aforementioned have provided verification data for studying the evapotranspiration at the traditional point scale. They enriched the theoretical research foundation for the river basin evapotranspiration and gradually realized the estimation of global evapotranspiration.

Studies have shown that about 65% of global precipitation returns to the atmosphere in evaporation and continues to participate in the water cycle. Therefore, the estimation of evaporation can determine regional water exchange and is the key to the closure of the regional water cycle. The global environmental change affects regional landscape patterns. Human activities further intensify the change of landscape patterns in the global environment by changing local land-use and landscape patterns. The landscape pattern change is not a simple one-to-one relationship with the driving factors but the result of the interaction of various factors. The complex mechanism of action between landscape patterns and the hydrological process is essential geoscience research and closely relates to the hydrological process. Human activities have significantly changed the most apparent type of area, leading to changes in evapotranspiration, such as vegetation coverage, surface roughness, leaf area index and surface albedo. They are affected by complex underlying surface conditions and climate changes, being challenging to estimate accurately. Ekwueme & Agunwamba (2020) found through statistical significance study that evaporation, sunshine hours, solar radiation and rainfall have little influence on annual runoff because they are not statistically significant. It can be inferred from the results that identifying the factors that control runoff change can enhance the understanding of long-term processes of climatic runoff. Therefore, it is of great significance for promoting the rational distribution of regional water resources to find out the spatio-temporal variation law of evaporation and to define the evaporation under different wetland landscape patterns and vegetation cover conditions. Evapotranspiration, as an index to characterize wetland ecological characteristics, can reflect the self-development and evolution ability of the wetland ecosystem and serve as the basis for ecological water supply and restoration and reconstruction of degraded wetlands in the reservoir area. It also provides a relevant reference basis for ecological restoration and reconstruction of degraded wetlands in the reservoir area to promote ecological conservation and biodiversity protection of wetlands in the Sanmenxia Reservoir area. Moreover, this study analyzes remote sensing inversion characteristics and driving factors of wetland evapotranspiration in the reservoir area on a large scale. Through literature research, it is found that there are few relevant studies considering human disturbance, which makes up for the deficiency of wetland research in the reservoir area to a certain extent.

The main body of this paper includes five parts: the introduction of the research area, the introduction of the research method, the results and analysis, the discussion and the conclusion.

2. PROFILE OF STUDY AREA

Located within the territory of Henan Province and Shanxi Province, the river basin in the Sanmenxia Reservoir area starts from Sanmenxia hydro-junction in the east, extends to the Weinan City of Shaanxi Province in the west, adjoins Pinglu and Ruicheng of Shanxi Province and the Tielian Mountain in Dali of Shaanxi Province in the north and leans against Yixiao Mountain and Xiaoqinling Mountain Range in the south (Figure 1). The Sanmenxia Dam at 20 km to the east of Sanmenxia

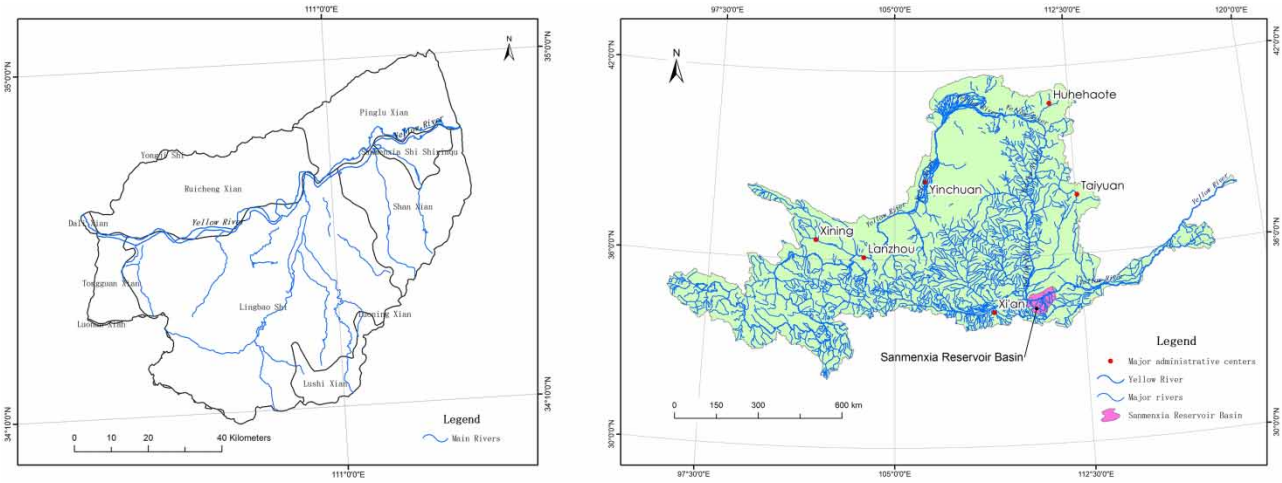

Figure 1 | Location and administrative division of river basin in the Sanmenxia Reservoir area.

City was used as the control node. The basin area is 688,400 km^2, accounting for 91.5% of the total area of the Yellow River basin. This river basin is in the intermountain (Zhongtiao Mountain and Qinling Mountains) basin. The Yellow River valley from the west of Sanmenxia (Henan) to Fenglingdu (Shanxi) is relatively wide, and its two banks are tableland formed by loess and plain on lower reaches of the Weihe River. The part from Jiamakou in Linyi County to Fenglingdu in Ruicheng County in Shanxi is a wandering-type silted river channel. The whole river basin is characterized by a semiarid continental monsoon climate, with uneven spatial and temporal distribution of precipitation. Specifically, precipitation is less in winter and spring, and a rainstorm is concentrated in summer and autumn. In this reservoir area, the annual average precipitation is 587 mm, and precipitation is mainly concentrated during July–September, accounting for 50% of the annual total precipitation. The annual average evaporation capacity is 2,221 mm, up to a maximum value of 2,665 mm.

3. METHODS

3.1. Data source and data preprocessing

The remote sensing data selected in this study were Landsat8 OIL_TIR from the United States Geological Survey (USGS) (http://earthexplorer.usgs.gov/). Two-period remote sensing images in the growing season of wetland plants were selected for a comparative analysis of changes. The images were acquired on July 7, 2014 and July 5, 2019, respectively, during which the cloud cover was small and surface plants expanded further.

After the remote sensing data were preprocessed through radiometric calibration, atmospheric correction and image fusion. We then chose eCognition, which is based on the object-oriented remote sensing image processing software, to segment the image with the multiresolution segmentation algorithm and classified the image's land use with the feature indexes of the image classification.

The selected meteorological data of Sanmenxia Meteorological Station within the river basin in 2014 and July 2019 were derived from the Meteorological Data Center of China Meteorological Administration (http://data.cma.cn/). The daily potential evapotranspiration capacities of Sanmenxia Meteorological Station throughout July were estimated by combining meteorological factors (i.e., wind velocity, air temperature, precipitation, temperature and humidity) with the latest corrected Penman–Monteith formula proposed by the Food and Agriculture Organization of the United Nations (FAO).

3.2. Basic principles of the SEBAL model

Tsanov *et al.* (2020) combine web and MATLAB. It is mentioned in the article that most methods to alleviate water pressure take into account the temporal and spatial characteristics of water resources and simulate practical problems by applying scientific knowledge rather than considering the problems as a whole. The SEBAL model is a monolayer model developed by Bastiaanssen (1995) based on the energy balance on the land surface to calculate latent heat flux. This model regards soil and vegetation as a whole and neglects the energy and material transport between vegetation and soil. It has been extensively applied to the remote sensing-based estimation of actual evapotranspiration under clear physical significance and high calculation accuracy. Zeng *et al.* (2008) described the SEBAL model-based remote sensing inversion of evapotranspiration in

detail using Landsat TM/ETM+ data, which guided the application of the SEBAL model in the evapotranspiration inversion. By optimizing the selection of cold and hot spots in the SEBAL model, Xia (Cheng & Brutsaert 2005) improved its inversion accuracy. With high vegetation coverage and relatively homogeneous overall terrain, the river basin in the Sanmenxia Reservoir area is suitable for evapotranspiration inversion *via* the SEBAL model.

In this study, the SEBAL model was applied for inverting some basic parameters, such as ground reflectivity, NDVI and surface emissivity within seven wavebands of Landsat8 OIL_TIRS multispectral data. Next, the inversion of surface temperature was conducted using the atmospheric correction method to operate the thermal infrared bands. Finally, the surface energy-balance equation was established by combining the meteorological data in the river basin:

$$R_n + G + H + \lambda \mathrm{ET} = 0 \tag{1}$$

where R_n is the net surface radiation flux ($\mathrm{W \cdot m^{-2}}$), G is the soil heat flux ($\mathrm{W \cdot m^{-2}}$), H is the latent heat flux ($\mathrm{W \cdot m^{-2}}$), λ is the latent heat of water vaporization ($\mathrm{W \cdot m^{-2} \cdot mm^{-1}}$) and ET is the evapotranspiration capacity (mm).

After calculating the major model parameters (R_n, G, H, λ and ET) in Equation (1), the constant evaporation ratio method was introduced to extend the instantaneous evapotranspiration on time scale to obtain the evapotranspiration capacity in 24 h. The technical process of SEBAL model-based evapotranspiration inversion is displayed in Figure 2.

3.3. Model and determination of important parameters

3.3.1. Net surface radiation flux: R_n

Net surface radiation flux, which serves as the primary energy source in the transport and exchange process of energy, momentum and moisture on the earth surface, reflects the relationship of solar shortwave radiation absorbed and reflected within the unit surface area with atmospheric long-wave radiation in the following formula:

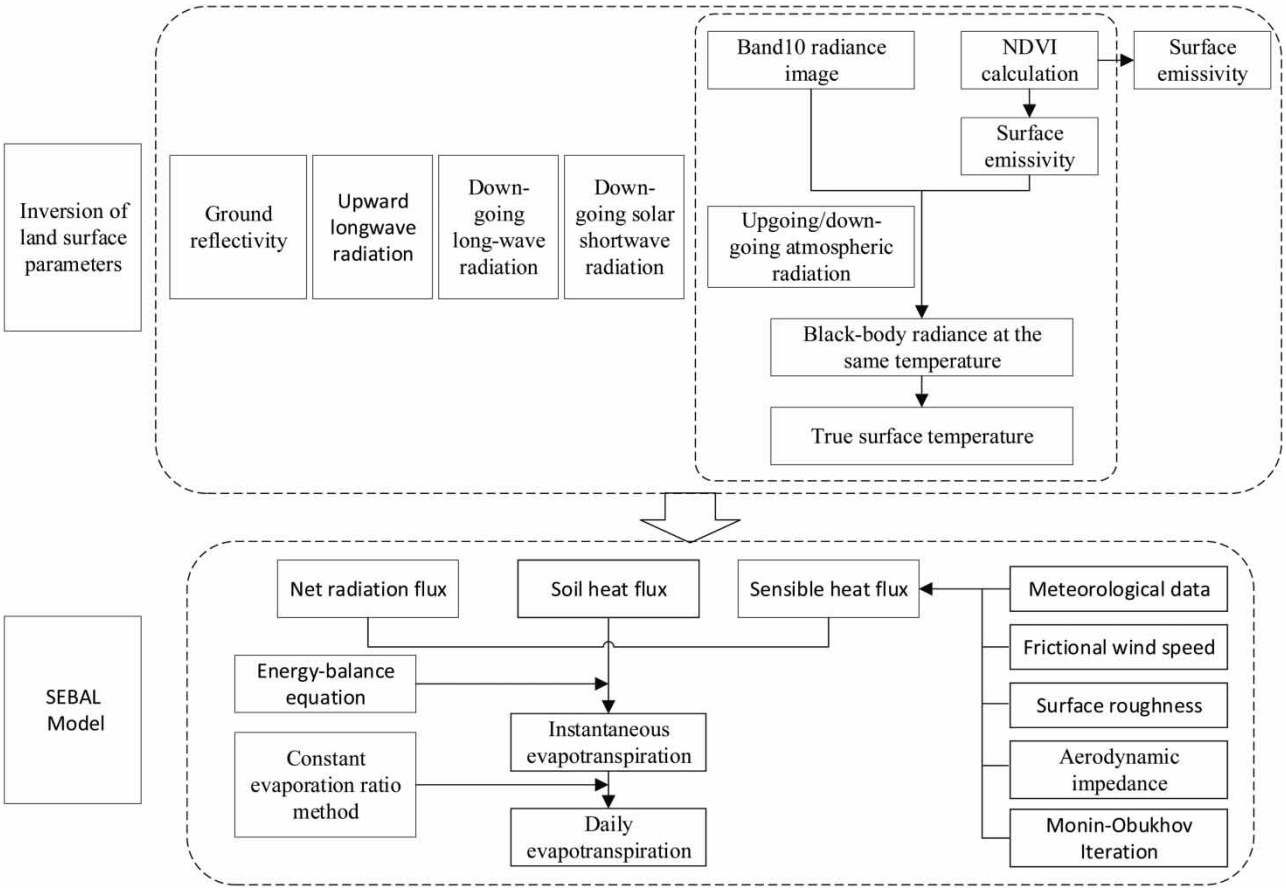

Figure 2 | Flowchart of the SEBAL model.

$$R_n = (1-\alpha)R_{s\downarrow} + R_{L\downarrow} - R_{L\uparrow} - (1-\varepsilon)R_{L\downarrow} \tag{2}$$

where α is the ground reflectivity, $R_{s\downarrow}$ is the down-going solar shortwave radiation, $R_{L\downarrow}$ is the down-going long-wave radiation, $R_{L\uparrow}$ is the upgoing long-wave radiation and ε is the surface emissivity.

3.3.2. Soil heat flux: *G*

Soil heat flux is the energy transferred by topsoil to deep soil in the form of heat conduction. Despite the small soil heat flux in comparison with R_n, H and λET, it plays a significant role in maintaining the energy balance (Bastiaanssen *et al.* 1998).

$$G = \frac{T_s - 273.16}{\alpha} \times \left| 0.0032 \times \frac{\alpha}{c_{11}} + 0.0062 \times \left| \frac{\alpha}{c_{11}} \right|^2 \right| \times (1 - 0.978\mathrm{NDVI}^4) \times R_n \tag{3}$$

where c_{11} denotes the influence of satellite transit time on G, and it is taken as 1.0 if the satellite transits through the territory at a local time of 12:00–14:00. NDVI is the normalized differential vegetation index, and T_s is the surface temperature (K), which is obtained through inversion using the atmospheric correction method.

3.3.3. Sensible heat flux: *H*

Sensible heat flux is the energy dissipated in the atmosphere during the near-surface thermal momentum transfer process. By combining parameters like wind velocity, surface roughness, air density and aerodynamic resistance, the Monin–Obukhov similarity theory (Cheng & Brutsaert 2005) was introduced to correct the aerodynamic resistance through multiple iterative operations until a steady H value was obtained.

$$H = \frac{\rho_{\mathrm{air}} C_p dT}{r_{\mathrm{ah}}} \tag{4}$$

where ρ_{air} is the air density ($\mathrm{kg \cdot m^{-3}}$), C_p is the heat constant in air (taken as $1{,}004\,\mathrm{J \cdot kg^{-1} \cdot K^{-1}}$; $dT = T_{0.01} - T_2$), $T_{0.01}$ represents the temperature at the height of 0.01 m, T_2 is the temperature at the height of 2 m and r_{ah} is the aerodynamic resistance ($\mathrm{s \cdot m^{-1}}$).

In the SEBAL model, dT presents the following linear relation with surface temperature:

$$dT = aT_s + b \tag{5}$$

In order to obtain stable a and b values in Equation (5), the energy and mass transfer process between the ground and air was simulated *via* the Monin–Obukhov similarity theory. In the SEBAL model, we took the image elements with sufficient moisture supply, complete vegetation coverage and low temperature as 'cold spots', and the high-temperature image elements without surface vegetation coverage as 'hot spots'. As the energy dissipated by cold-spot image elements from the surface to the atmosphere was nearly 0, $H = 0$, and as the evapotranspiration capacity of hot-spot image elements was nearly 0, $\lambda\mathrm{ET} = 0$. The intense subjectivity in selecting 'cold spots' and 'hot spots' significantly impacted the inversion accuracy. Based on the above assumption, stable values of a, b, r_{ah} and H were obtained through the loop iterative calculation of Monin–Obukho length, namely, $L = -\rho_{\mathrm{air}} C_p u^{*3} T_s / KgH$ (u^* is the friction velocity under neutral stability).

3.3.4. Calculation of evaporation ratio and evapotranspiration capacity

According to the constant evaporation ratio method principle, the ratio (namely instantaneous evaporation ratio Λ) of latent heat flux to the difference value between net surface radiation flux and sensible heat flux within a day is stable (Harrison 1963). The evaporation ratio can be calculated using the following formula:

$$\Lambda = \frac{\lambda\mathrm{ET}}{R_n - G} = \frac{R_n - G - H}{R_n - G} \tag{6}$$

The latent heat flux in 24 h are given by the following equation:

$$\lambda ET_{24} = \Lambda\ (R_{n24} - G_{24}) \tag{7}$$

The evapotranspiration capacity in 24 h can be estimated using the following equation:

$$ET_{24} = \frac{86,\ 400\Lambda\ (R_{n24} - G_{24})}{\lambda} \tag{8}$$

where G_{24} can be ignored in the estimation of the evapotranspiration capacity in 24 h.

λ is the latent heat of water vaporization (J/kg) (Harrison 1963), and its calculation formula is as follows:

$$\lambda = (2.501 - 0.002361(T_s - 273.15)) \times 10^6 \tag{9}$$

R_{n24} is the daily net radiation flux (W/m^2), and it can be calculated using the following formula:

$$R_{n24} = (1 - \alpha)R_{a24} - 110\tau_{sw} \tag{10}$$

$$R_{a24} = \frac{G_{sc}}{\pi \times d_r}[w_s\ \sin\emptyset\ \sin\delta + \cos\emptyset\ \cos\delta\ \sin w_s] \tag{11}$$

$$w_s = \arccos[-\tan\emptyset\ \tan\delta] \tag{12}$$

$$\delta = 0.409\sin\left(\frac{2\pi}{365}J - 1.39\right) \tag{13}$$

where G_{sc} is the solar constant (1,367 W/m^2), d_r is the relative sun-to-earth distance, $\emptyset$ is the geographic latitude of the image element (rad) and δ is the solar declination.

3.4. Model verification *via* the Penman–Monteith formula

To verify the accuracy of the SEBAL model, the FAO Penman–Monteith formula was used to verify the potential evapotranspiration at Sanmenxia Meteorological Station. That formula is as follows:

$$ET_0 = \frac{0.408\Delta(R_n - G) + \gamma\frac{900}{T + 273}u_2(e_s - e_a)}{\Delta + \gamma(1 + 0.34u_2)} \tag{14}$$

where ET_0 is the potential evapotranspiration capacity (mm/d), R_n is the net surface radiation (MJ/(m^2 · d)), γ is the psychrometer constant (KPa/°C), u_2 is the wind velocity at the height of 2 m, e_s is the saturation vapor pressure (KPa), e_a is the actual vapor pressure (KPa) and Δ is the slope of saturation vapor pressure–temperature relation curve (KPa/°C).

Based on the verification data in 2014 and Equation (14), the potential evapotranspiration capacity at Sanmenxia Meteorological Station in the same period was calculated as 5.032 mm. By contrast, the result obtained through the SEBAL model inversion was 4.66 mm at the meteorological station. The error was 7.39% and not large. Hence, obtaining the evapotranspiration capacity in this area through the SEBAL model inversion is quite reliable.

4. RESULTS AND DISCUSSION

4.1. Results

4.1.1. Spatial distribution characteristics of evapotranspiration capacities in different land-use types

The land-use types in the Sanmenxia river basin include artificial wetland, urban land, farmland, beach land, forest land, grassland, lake, marsh wetland and river (Yi 2013). The total area of Sanmenxia river basin is 5,999.48 km^2, and the total wetland (including artificial wetland, beach land, lake, marsh wetland and river) areas in 2014 and 2019 were 150.37 and 166.42 km^2, respectively, accounting for 2.5 and 2.77% of the total basin area, respectively. The total non-wetland (urban

land, farmland, forest land and grassland) areas were, respectively, 5,849.54 and 5,838.30 km^2, accounting for 97.5 and 97.23% of the total basin area as shown in Figure 3(a).

Affected by soil moisture status, meteorological factors, vegetation growth, the daily evapotranspiration capacities in different land-use types within the whole study area in 2014 and 2019 were 0–10.61 and 0–13.392 mm/d, respectively. In 2014, the daily average evapotranspiration capacities in descending order were lake (10.61 mm/d), river (9.33 mm/d), forest land (8.91 mm/d), artificial wetland (8.11 mm/d), marsh (8.07 mm/d), beach land (6.43 mm/d), grassland (5.30 mm/d), farmland (3.40 mm/d) and urban land (2.71 mm/d). In 2019, the daily average evapotranspiration capacities in descending order were river (13.49 mm/d), lake (13.25 mm/d), forest land (9.91 mm/d), marsh (9.60 mm/d), artificial wetland (9.44 mm/d), beach land (9.09 mm/d), grassland (6.01 mm/d), farmland (5.36 mm/d) and urban land (4.82 mm/d). The daily evapotranspiration distributions in the entire study area are shown in Table 1 and Figure 4(a) and 4(b).

4.1.1.1. Urban land. Wang *et al.* (2017) found that urbanization changed the landscape pattern of wetlands, resulting in a continuous decrease in wetland area, landscape fragmentation, increased heterogeneity and decreased connectivity of wetlands. Urbanization also changes the hydrological conditions of wetlands, weakens the natural regulation and storage capacity, strengthens the runoff coefficient, increases the flood peak discharge and aggravates soil erosion. This study area is located within the territory of Sanmenxia City, and many cities and towns are distributed along the Yellow River. The urban land area in 2019 was increased by 7.36 km^2 in comparison with that in 2014. The daily average evapotranspiration capacity was 2.11 mm/d higher than that in 2014, driven by the high-temperature weather in July 2014 (with daily average temperature of up to 37.5 °C) relative to that in 2019.

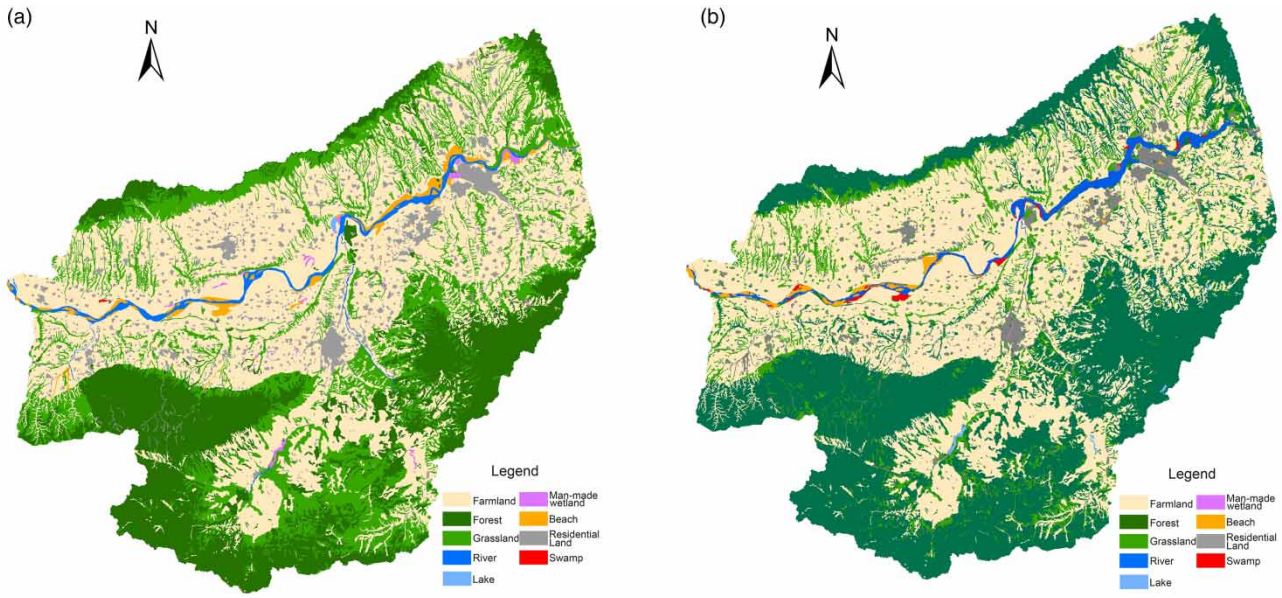

Figure 3 | Land-use types in the Sanmenxia river basin in July 2014 (a) and land-use types in the Sanmenxia river basin in July 2019 (b).

Table 1 | Daily average evapotranspiration capacities of wetlands and non-wetlands (mm/d)

		Wetland					Non-wetland			
Year	Item	Lake	River	Artificial wetland	Beach land	Marsh	Forest land	Farmland	Urban land	Grassland
2014	Area (km^2)	9.16	83.00	1.17	46.39	10.64	2,090.28	2,657.46	233.71	868.08
	Daily evapotranspiration	10.61	10.33	8.11	6.43	8.07	8.31	3.40	2.71	5.30
2019	Area (km^2)	9.32	87.19	1.26	29.18	12.50	2,402.93	2,658.18	241.065	557.84
	Daily evapotranspiration	13.25	13.49	9.44	9.09	9.60	9.91	5.36	4.82	6.01

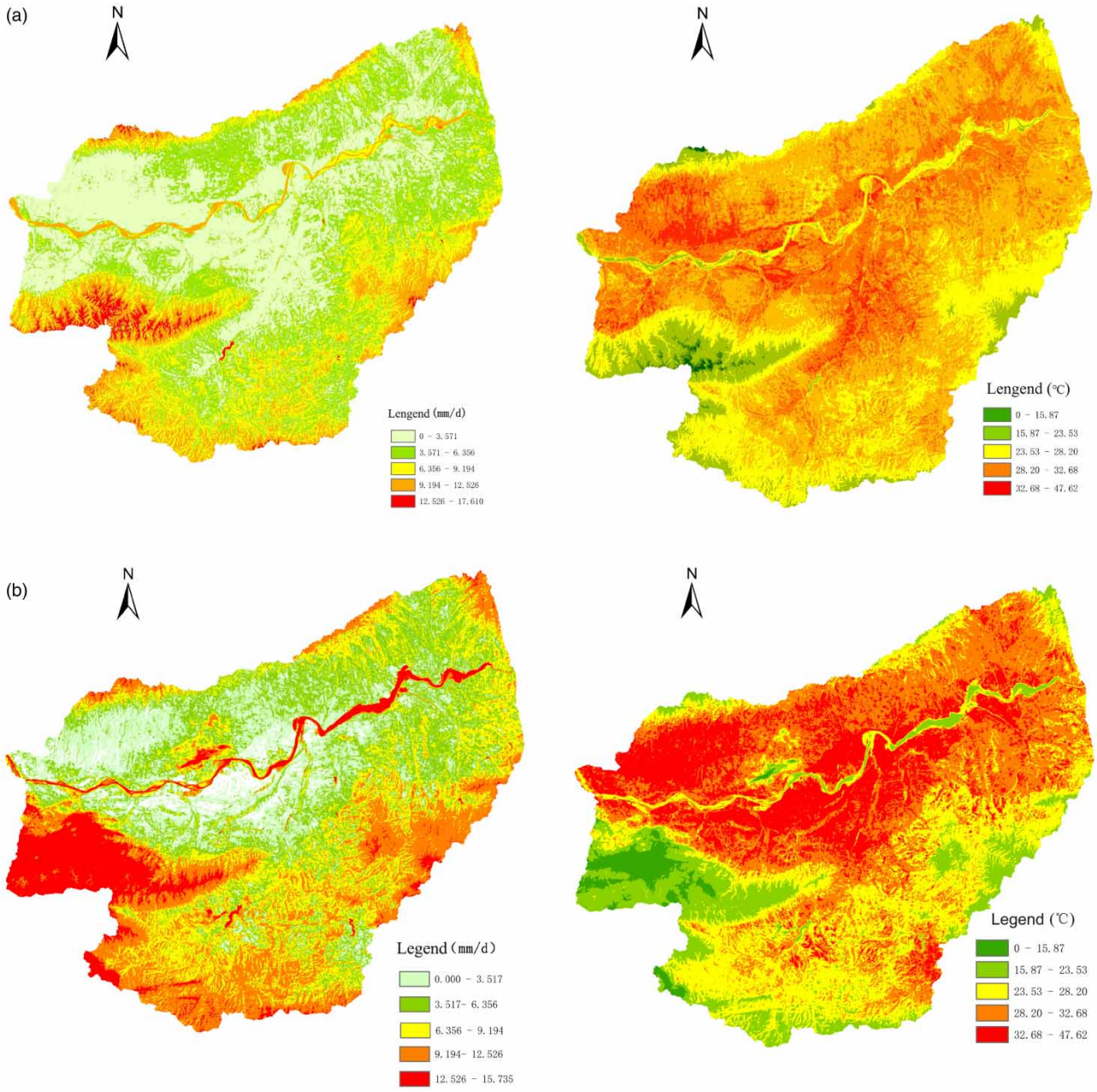

Figure 4 | (a) Evapotranspiration capacity surface temperature in the Sanmenxia river basin in July 2014. (b) Evapotranspiration capacity surface temperature in the Sanmenxia river basin in July 2019.

4.1.1.2. Forest land, farmland and grassland. Cao *et al.* (2017) found that the spatial distribution characteristics of forest evapotranspiration contribution in four seasons were significant. High temperature, abundant precipitation and sufficient light in summer were the periods of vigorous growth of forest land and the highest evapotranspiration contribution of forest land in a year occurred in summer. The maximum contribution value of farmland to annual evapotranspiration is also in summer when the crop coefficient reaches the maximum, and the opposite is true in winter.

Forest land is mainly located in the northern and southern mountainous areas in the study area. The daily average evapotranspiration capacities in 2014 and 2019 were 8.31 and 9.91 mm/d, respectively. The agricultural production area is mainly distributed in flat zones on the north and south of the Yellow River, covering approximately 7.86% of the total basin area. The daily average evapotranspiration capacities of the agricultural production area in 2014 and 2019 were 3.40 and 5.36 mm/d, respectively. Grasslands presented dispersed distribution in the study area; the northern grassland patch area was large, while

the southern grassland patch area was small. The daily average evapotranspiration capacities in 2014 and 2019 were 5.30 and 6.01 mm/d, respectively.

4.1.1.3. River and lake. Cui *et al.* (2021) found that the annual average actual evapotranspiration, vegetation transpiration and vegetation evaporation after water storage under artificial regulation were increased compared with those before water storage. On the other hand, ground evaporation decreased after water storage compared with before water storage. In addition, Zhou *et al.* (2014) found that among the changes of many climate factors, precipitation is the key factor to maintain the water quantity of wetland, and the decrease of precipitation will obviously intensify the shrinkage of wetland area, and even change the wetland type. The main river within this river basin is the Tongguan-Sanmenxia section of the Yellow River. Affected by the water-level regulation and precipitation of Sanmenxia hydro-junction, the river area (about 1.45% of the total basin area) changed little in 2014 and 2019. The daily average evapotranspiration capacities in 2014 and 2019 were 10.33 and 13.49 mm/d, respectively.

Lake is an important part of the wetland ecosystem. The lakes in the study area mainly include Dinghu Bay and Taijisheng Lake, accounting for about 0.16% of the total basin area. The main vegetation types are *Phragmites australis* (Cav.) *Trin. ex Steud* and *Typha angustifolia*. The daily average evapotranspiration was only second to that of the river wetland landscape, being 10.61 and 13.25 mm/d in 2014 and 2019, respectively.

4.1.1.4. Beach land, marsh and artificial wetland. Lv *et al.* (2018) found that the wetland area in the Beijing-Tianjin-Hebei region showed a decreasing trend in the past 30 years, and the wetland area change showed a trend from a slight increase to a rapid decrease. Among the five types of natural wetland, the area of lakes and channels increased, while the area of tidal flats, tidal lands and marshland decreased. The main reasons for the impact are the rapid growth of population and economy and other factors, and the regions with serious wetland damage also show differences on time scale. Beach land is located at the two banks of the river and the river island, including the hydro-fluctuation belt generated due to the water-level change in the reservoir area. Influenced by the water-level regulation in Sanmenxia hydro-junction, large areas of beach lands were formed along the Yellow River, and their unique geographical location and hydrologic process have contributed to unique wetland soil and vegetation landscapes. The inversion results show that the reservoir regulation significantly affected the beach land area, but the less disturbed by human activities. The beach land accounted for about 0.49% of the total basin area, and the daily average evapotranspiration capacities in 2014 and 2019 were 6.43 and 9.09 mm/d, respectively.

As important wetland types, marsh and beach land are interchangeable with the water-level variation in the reservoir area. The marshland within the river basin is mainly distributed along the river, with the main vegetation community of *P. australis (Cav.) Trin. ex Steud*, and its area is 0.2% or so of the total basin area. The marsh area is affected by the changes of the river's main current to a great extent. Yi (2013) believed that the rechanneling and diversion of river, in particular, have changed the physiochemical properties and hydrological conditions of soil, thus affecting the vegetation succession of marsh wetland. Located in a densely populated area, the marsh wetland in the Sanmenxia river basin is greatly disturbed by human activities. Under the dual impacts of water surface evaporation and plant transpiration, the daily average evapotranspiration capacities in 2014 and 2019 were 8.07 and 9.60 mm/d, respectively.

In the river basin, the artificial wetlands include reservoirs, pit ponds and canals, most of which concentrate on aquaculture and embody the human disturbance to nonnatural wetlands, and the artificial wetlands account for about 0.021% of the total basin area. The daily average evapotranspiration capacities in 2014 and 2019 were 8.11 and 9.44 mm/d, respectively.

4.1.2. Study of factors driving the evapotranspiration process

The evapotranspiration process in the basin is affected by many factors. For instance, the changes in meteorological conditions, solar radiation and hydrologic processes can significantly alter the potential evaporation of the underlying surface in an area and influence the water deprivation due to the evapotranspiration in the basin. This can modify the production and domestic water-use pattern of the whole basin (Yuan *et al.* 2012). The analysis indicates that:

1. According to some previous evapotranspiration studies (Zeng *et al.* 2008; Liu *et al.* 2009; Zhang 2011, 2013; Li *et al.* 2012), the daily evapotranspiration capacity in the water area (lake and river) was the highest. However, in the evapotranspiration results in July 2014 and July 2019, the daily evapotranspiration capacity of the water area often exceeded that of

artificial wetland. This was because the artificial wetland was dried up, and the wetland vegetations experienced poor growth status and even withered due to the persistent drought. Therefore, by comparing the differences of water area and other land-use types (beach land, marsh and artificial wetland) in evapotranspiration, we deduce that the water surface area is one of the driving factors influencing evapotranspiration.

2. The main reasons why the daily evapotranspiration capacity of urban land and grassland was higher than that of farmland were as follows. First, there were a small quantity of green belts and woods in the urban area in the land-use classification. Thus, the evapotranspiration capacity obtained through the inversion was high. Second, the main crop planted in the agricultural region of the Sanmenxia basin is winter wheat, and following the last 10 days of May when winter wheat enters the heading stage is the most critical period for its growth with high water demand. Nevertheless, the precipitation was relatively small after July 2019, so the overall crop growth in the whole area was poor, and the difference between grassland and farmland in daily average evapotranspiration was quite small due to drought. However, the vegetation type of farmland is simple, mainly being wheat, and the primary vegetation type in grassland is bush, with a relatively high vegetation diversity. The difference between the two land-use types in the evapotranspiration manifests that the plant diversity and their growth status in the area constitute one of the driving factors influencing the evapotranspiration.
3. The study shows that surface temperature and vegetation coverage in the river basin are key factors influencing the evapotranspiration process. The daily average evapotranspiration capacity of forest land was close to wetlands (e.g., marsh, beach land and artificial wetland). Meanwhile, its value was about twice those of farmland and grassland. By analyzing the surface temperatures (Figure 3(c)) obtained through the remote sensing inversion in 2019, it is shown that farmland and grassland were areas with high surface temperatures (both exceeded 23.5 °C), while the areas with low surface temperatures (below 23.5 °C) mainly appeared in the southeast mountainous area, with forest land being the primary land-use type. By comparing the surface temperature results in July 2014, the average surface temperatures of both farmland and grassland were over 37.7 °C, and that of forest land was 32.1 °C. This indicates that surface temperature is the primary factor influencing the evapotranspiration process, and the evapotranspiration capacity is relatively small in the area with relatively high surface temperature. In addition, the vegetation coverage of forest land within the mountainous area is higher than that of farmland and grassland. The dense forest and favorable vegetation growth can facilitate the evapotranspiration of forest land, which is consistent with the conclusion of Gu *et al.* (2021).

4.2. Discussion

4.2.1. Comparative analysis of wetland landscapes and non-wetland landscapes in evapotranspiration capacity

The remote sensing images in both periods reflect that the evapotranspiration capacity of wetland landscapes is higher than that of non-wetland landscapes. According to the evapotranspiration results obtained from remote sensing in this area in 2019, the daily average evapotranspiration capacity corresponding to different landscape types could be divided into three gradient ranges: 4.82–6.01 mm/d (farmland, urban land and grassland), 9.09–9.91 mm/d (artificial wetland, beach land, marsh and forest land) and 13.25–13.49 mm/d (lake and river). Except for forest land, the daily average evapotranspiration capacity of all wetland types was greater than 9.09 mm/d, and that of all non-wetland types was smaller than 6.01 mm/d. In the whole river basin, wetland's daily average evapotranspiration capacity was 12.17 mm/d, while that of non-wetland was 7.26 mm/d (accounting for only 59.7% of the former), indicating a great difference between the two land-use types (Figure 5). A similar feature was manifested in the remote sensing inversion results in the same period in 2014, the daily average evapotranspiration capacity of wetland was 8.71 mm/d and that of non-wetland was 4.93 mm/d, accounting for merely 56.6% of the former (Figure 5).

By comparing the daily evapotranspiration results in July 2014 and July 2019, wetland landscapes' overall daily average evapotranspiration capacity in 2014 was 3.46 mm/d which was lower than that in 2019. On the other hand, the daily evapotranspiration capacity of non-wetland landscapes in July 2014 was 2.33 mm/d which was smaller than that in July 2019. Overall, the daily evapotranspiration of wetland landscapes was higher than that of non-wetland landscapes, and the latter was approximately 60% of the former.

The evapotranspiration capacity of wetland landscapes is higher than that of non-wetland landscapes because of sufficient water supply to wetland vegetations, i.e., the higher the temperature (within a certain range of threshold) is, the faster the evapotranspiration process will be. The area of lakes and rivers in the Sanmenxia basin accounts for 67.5% of the total wetland area, and the broad water surface area has accelerated the evapotranspiration process and facilitated the hydrologic cycle of the whole wetland ecosystem. This resulted in a relatively high evapotranspiration capacity of wetland landscapes.

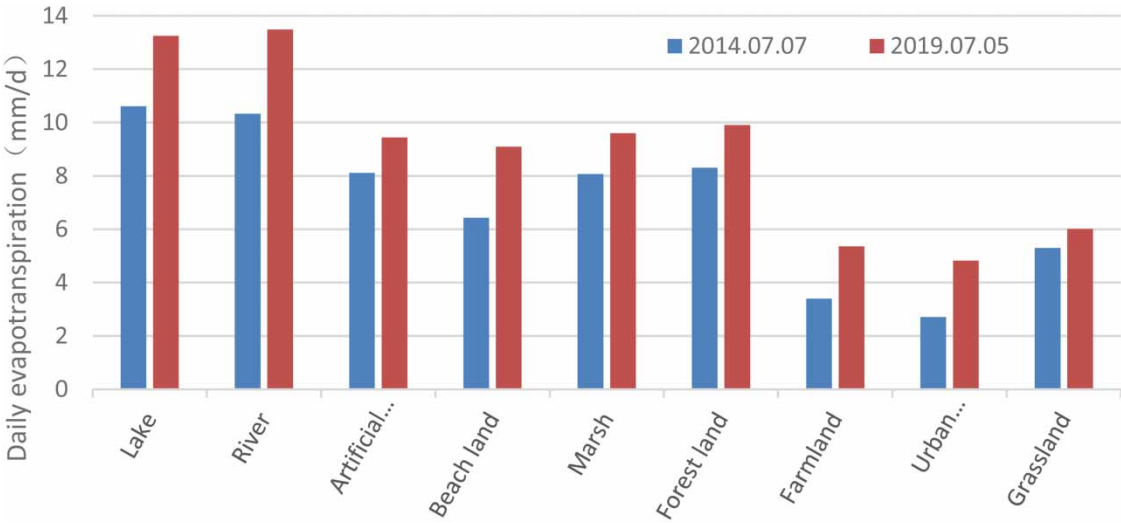

Figure 5 | Comparison of daily evapotranspiration capacity for wetland landscapes and non-wetland landscapes.

4.2.2. Evapotranspiration difference analysis under landscape patterns in different periods

Based on a comparison of area changes of landscape types in 2014 and 2019, we found that the area changes of farmland, urban land, artificial wetland and marsh were little, but the areas of forest land and grassland changed to the greatest extent. In addition, they experienced mutual transformation. In the southwest and northern mountainous areas, the forest land area in 2019 was 312.65 km^2 more than that in 2014, while the grassland area was 310.24 km^2 less than that in 2014. Influenced by the water-level regulation of the Sanmenxia hydro-junction project (Mao *et al.* 2006; Wang *et al.* 2011), the areas of beach land and river wetland along the river on the lower reaches of the reservoir were mutually transformed. Namely, partial beach land was gradually converted into grassland and marsh.

By analyzing the evapotranspiration inversion results in the same month of the two periods, it can be found that the evapotranspiration of forest land was higher than that of grassland, while that of river was higher than that of beach land. This indicates that the evapotranspiration capacity of different surface features is unrelated to their areas but correlated with land cover and soil texture. The evapotranspiration capacities of all surface features in July 2014 were lower than those in July 2019. Specifically, the evapotranspiration changes of river, lake, beach land and urban land were the most obvious. However, the relative difference values among marsh, forest land and grassland were small. They reflect that other than soil moisture status and meteorological factors (e.g., daily average air temperature), the evapotranspiration capacity is also greatly affected by the interannual variation of vegetation cover characteristics, which is consistent with the conclusion of Chen & Zeng (2013).

5. CONCLUSIONS

The daily evapotranspiration capacities of wetlands and non-wetlands in the Sanmenxia river basin were quantitatively estimated *via* the SEBAL model, and the remote sensing inversion results were verified using the FAO Penman–Monteith formula. The verification results demonstrate that the SEBAL model is relatively accurate and feasible in studying evapotranspiration in the Sanmenxia river basin.

Significant differences exist between wetland landscapes and non-wetland landscapes in different land-use types in the aspect of evapotranspiration capacity. The daily average evapotranspiration capacities of river and lake are the highest, followed by those of forest land, marsh, beach land and artificial wetland, and then those of grassland, urban land and farmland. The non-wetland landscapes (forest land, grassland, farmland and urban land) account for 97.23% of the total basin area, with the daily average evapotranspiration capacity of only 7.26 mm/d. On the other hand, the wetland landscapes (river, lake, marsh, beach land and artificial wetland) account for 2.77% of the total basin area, with the daily average evapotranspiration capacity of 12.17 mm/d. In a sense, the daily evapotranspiration capacity of the non-wetland area is about 59.7% of the wetland area.

Beyond meteorological, hydrological and solar radiation factors, the interannual variations of water surface area, vegetation diversity, vegetation growth status and vegetation coverage, along with surface temperature, are also important driving factors of wetland evapotranspiration.

It is worth mentioning that using remote sensing to estimate evapotranspiration of wetlands has important scientific significance:

1. Evapotranspiration (ET) includes the evaporation of water from the surface and plant surfaces and the transpiration of water through the surface and inside plants, which is an essential part of the hydrological cycle. At the same time, evaporation and evapotranspiration are also the main heat balance items because changing water into gas requires heat absorption. Surface heat and water balance largely determine the composition and evolution of geographical environment. A clear evapotranspiration process is helpful to understand the energy balance and water cycle. At the same time, it also helps to correctly assess the impact of climate and human activities on farmland ecosystems.
2. Wetland is an essential part of the ecosystem. Wetland hydrological process controls the biological and chemical processes of wetland which is the most important factor affecting the function and evolution of wetland. Evaporation is an essential part of the wetland water cycle. Water loss is the leading way to correspond with evaporation. The latent heat flux is the primary energy expenditure wetland evaporation, so to speak to a great extent, affecting the wetland water heat balance for the wetland system. We investigated its relationship between rainfall and evaporation, quantitative estimation of evaporation amount. It has health significance to the whole wetland ecosystem.
3. Rapid acquisition of evapotranspiration from remote sensing is of great significance for ecosystem protection, which also helps decision-makers to make rapid judgments.

ACKNOWLEDGEMENTS

This work was supported by the National Natural Science Foundation of China (NSFC) Program (Nos 51679256 and 51179207), the Major National Science and Technology Program of Water Pollution Control and Governance (No. 2018ZX0711103), the Science and Technology Program of China Institute of Water Resources and Hydropower Research (Nos WE0145B012021 and WE0163A052018) and the Open Research Fund of Guangxi Key Laboratory of Water Engineering Materials and Structures, Guangxi Institute of Water Resources Research (No. GXHRI-WEMS-2020-13).

CONFLICT OF INTEREST

No conflict of interest exits in the submission of this manuscript.

DATA AVAILABILITY STATEMENT

All relevant data are included in the paper or its Supplementary Information.

REFERENCES

Allen, R. G., Pereira, L. S. & Raes, D. 1998 *Crop Evapotranspiration – Guidelines for Computing Crop Water Requirements*. FAO Irrigation and Drainage Paper 56. FAO, p. 56.

Bastiaanssen, W. 1995 *Regionalization of Surface Flux Densities and Moisture Indicators in Composite Terrain: A Remote Sensing Approach Under Clear Skies in Mediterranean Climates*. Wageningen Agriculture University, Netherland, p. 273.

Bastiaanssen, W. G. M., Menenti, M., Feddes, R. A. & Holtslag, A. A. M. 1998 A remote sensing surface energy balance algorithm for Land (SEBAL) 1. Formulation. *Journal of Hydrology* **212–213**, 198–212.

Cao, Y., Gao, L. & Guo, M. 2017 Characteristics of evapotranspiration for different types of land use in Liaoning Province. *Advances in Science and Technology of Water Resources* **37** (02), 14–19.

Chen, H. & Zeng, X. 2013 Impact of vegetation interannual variability on evapotranspiration. *Acta Ecologica Sinica* **33** (14), 4343–4353.

Cheng, Y. M. B. & Brutsaert, W. 2005 Pathology of Monin-Obukhov similarity in the stable boundary layer. *Journal of Geophysical Research* **110** (D6), 25.

Cui, H., Wang, L. C., Wang, H. J., Xiao, W. H., Hou, B. D. & Gao, B. 2021 Temporal and spatial changes of actual evapotranspiration and its relationship with meteorological factors in the Three Gorges Reservoir area. *Research of Soil and Water Conservation* **193** (04), 202.

Ekwueme, B. N. & Agunwamba, J. C. 2020 Modeling the influence of meteorological variables on runoff in a tropical watershed. *Civil Engineering Journal* **6** (12), 2344–2351.

Gu, J., Xue, H., Dong, G., Zhou, L., Li, J., Dang, S. & Li, S. 2021 Effects of NDVI/land-use on spatiotemporal changes of evapotranspiration in the Yellow River Basin. *Arid Land Geography* **44** (01), 158–167.

Harrison, L. P. 1963 Fundamental concepts and definitions relating to humidity. In: *Humidity and Moisture*, Vol. 3 (Wexler, A., ed.). Reinhold Publishing Company, New York.

Li, H., Wang, H., Kong, Y. & Li, L. 2012 Estimation of evapotranspiration in Yellow River delta wetland based on two-source energy balance (TSEB) model. *Remote Sensing Technology and Application* **01**, 58–67.

Liu, C., Gao, W. & Gao, Z. 2009 Estimation of regional surface evapotranspiration using MODIS products. *Advances in in Water Science* **06**, 782–788.

Liu, M., Hu, D., Yu, C. & Wang, S. 2020 Temporal and spatial change characteristics of growing season evapotranspiration its cause analysis in Liaohe River delta wetland, China. *Acta Ecologica Sinica* **40** (02), 701–710.

Lv, J., Jiang, W., Wang, W., Chen, K., Deng, Y., Chen, Z. & Li, Z. 2018 Wetland landscape pattern change and its driving forces in Beijing-Tianjin-Hebei region in recent 30 years. *Acta Ecologica Sinica* **12**, 4492–4503.

Mao, Z., Peng, W., Wang, S. & Zhou, H. 2006 Study on effects of water level variation of the Sanmenxia reservoir on wetland hydrological processes. *Journal of China Institute of Water Resources and Hydropower Research* **01**, 36–41.

Tsanov, E., Ribarova, I., Dimova, G., Ninov, P. & Makropoulos, C. 2020 Water stress mitigation in the Vit River basin based on WEAP and Matlab simulation. *Civil Engineering Journal* **6** (11), 2058–2071.

Wang, X., Wang, J., Ge, Y. & Zhang, P. 2011 Environmental impact analysis on shore groundwater in the case of low water level of Sanmenxia Reservoir. *Yellow River* **10**, 39–41.

Wang, J.-Y., Han, Y.-P., Liu, L.-L., Wang, L., Bing, L.-F., Yin, Y. & Xi, F.-M. 2017 Progress in studies of the impacts of urbanization on wetland. *Science & Management* **13** (03), 61–65.

Wu, W. 2016 Estimation and discussion of regional evapotranspiration in Anhui Province based on remote sensing model. In: *The 33rd Annual Meeting of the Chinese Meteorological Society S21 Development and Application of new Generation Meteorological Satellite Technology*. Chinese Meteorological Society, p. 4.

Yi, W. 2013 *A Study of Changes on Landscape Pattern and Driving Factors of Wetland in Sanmenxia Area Based on Remote Sensing*. China University of Geosciences, Beijing (S2), 88.

Yuan, Y., Yan, D., Jia, Y. & Hu, D. 2012 The impact of scale change of land use on evapotranspiration in Nenjiang River basin. *Journal of Hydraulic Engineering* **43** (12), 1440–1446.

Zeng, L., Song, K., Zhang, B. & Du, J. 2008 Retrieval of evapotranspiration in Zhalong wetland based on SEBAL model. *Agrometeorology of China* **04**, 420–426.

Zhang, D. 2011 SEBAL Model Improved and Study on the Relationship between ET and luce. Beijing Forestry University, Beijing.

Zhang, X. 2013 Estimation of evapotranspiration in wetland and surrounding area of Poyang Lake based on remote sensing technology. In: *Proceedings of the Annual Conference – S2 Lake Management, Development and Protection*. Chinese Hydraulic Engineering Society, p. 8.

Zheng, Q.-q., Dai, P.-c., Zhang, J.-y. & Wu, Z.-p. 2020 Evapotranspiration in the Jinghe River Basin based on the surface energy balance system. *Arid Zone Research* **37** (06), 1378–1387.

Zhou, B., Yin, J., Jin, B. & Zhu, L. 2014 Degradation of Wuchsng Lake wetland and its causes during 1980–2010. *Acta Geographica Sinica* **11**, 1697–1706.

First received 23 June 2021; accepted in revised form 17 September 2021. Available online 7 October 2021